

# Cross-fault Geology Characterization using Transient Electromagnetics

Aljawharah Alangari and Nicholas Dorogy, Colorado School of Mines

## SUMMARY

Steamboat Springs, CO, displays unique, relatively unstudied geological features along the Howelsen Ski Area fault. Discrepancies in cross-fault geology and mineral/hot spring compositions have raised questions about near-subsurface geology and layering. Transient Electromagnetic (TEM) soundings provide information about the magnetic field variation which, after inversion, produces resistivity vs depth information that is useful in interpreting local geology and identifying subsurface layering. Here we show that near-subsurface layering across the fault is highly correlated, but a more recent alluvial deposition on the foot wall is likely the cause of differences in surface geology and spring composition. We suggest a two-layer structure on the hanging wall, and a three-layer structure on the foot wall in which the lower two layers of the foot wall correspond to the two layers observed in the hanging wall.

## INTRODUCTION

Steamboat Springs lies in the Northwest quadrant of Colorado amid the Park Range Formation. A normal fault bisects the western edge of downtown steamboat and numerous mineral and hot springs are located along this formation (see figure 1). Despite the close proximity of these springs (in some cases no more than 10 m apart), significant differences in their chemical and mineral compositions exist. Moreover, previous studies have shown that cross-fault surface geology differs substantially in age and structure (Christopherson, 1997). These differences are directly attributable to the fault which influences the upwelling of water in the springs and controls erosional effects in the valley. Colorado School of Mines students collected TEM soundings in May of 2022 and 2023 in an effort to better understand near-subsurface geology along the fault. We invert these soundings to calculate subsurface resistivity at depth which we use to characterize layering and rock types. Our interpretations are used to improve our understanding of cross-fault lithology and differences in spring composition in the Steamboat area.

## METHODS

### Theory

#### Survey Design

Geophysics students from Colorado School of Mines recorded a total of 22 TEM soundings in Steamboat Springs in 2022 and 2023. Fifteen surveys were located on the hanging wall of the fault, while the remaining seven locations were located on the foot wall. Figure 1 depicts the locations of these sites shown as black symbols.

Every survey conformed to the same sampling parameters out-

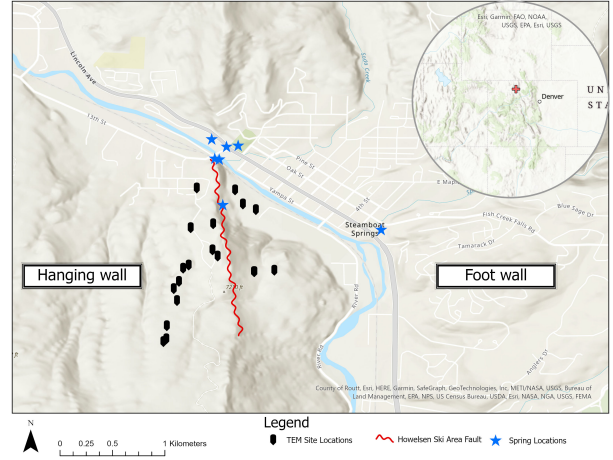


Figure 1: TEM survey, spring, and fault locations in the Steamboat Springs area.

lined in Appendix A. We then processed field data using the Aarhus SPIA software package (Aarhus SPIA Development Team, 2023).

### Processing

SPIA is a data processing and inversion software that allows the user to adjust initial model parameters and incorporate a prior information. Noise and spike filtering using ambient noise recording during data collection are automatically performed when data is uploaded. We manually remove erroneous data points that displayed clear deviation from the data trend. For each TEM sounding dataset, we created a prior model that best reduced initial data misfit by manually adjusting the number of layers present, and the depth and resistivity of these layers. Appendix B provides an example of the individual inversion results produced in SPIA.

After we produced individual inversions for every survey location, we divided our results into two groups. The first group consisted only of survey locations that lie on the hanging wall, whereas the second group was comprised only of surveys from the foot wall. We then calculated a single inversion for each side of the fault by averaging the individual inversions from the respective groups.

Moreover, because we noticed an abundance of water near the surface during survey acquisition, we use Archie's equation,

$$S_w^n = \frac{a \cdot R_w}{\phi^m \cdot R_t} \quad (1)$$

where:

- $a$ ,  $m$ , and  $n$  are constants commonly expressed as  $a = 1$ ,  $m = 2$ , and  $n = 2$  (AAPG Wiki, 2023).

## Yampa Valley Cross-fault Geology

- $R_f$  is the bulk resistivity of the formation.
- $R_w$  is the resistivity of water.
- $\phi$  is the bulk porosity of the formation.
- $S_w$  is the water saturation of the formation.

to constrain potential rock types by calculating porosities based on estimates of the resistivity of local water, water saturation, and our measured resistivities (Archie, 1952). By accounting for both resistivity and porosity measurements, we are able to more discretely estimate potential rock types and thus suggest a more accurate interpretation of the local geology.

### RESULTS

We calculated averaged inversions, as shown in Figure 2, to reduce the effects of localized magnetic field anomalies that may affect our results. Our cross-fault averaged inversions produced a three-layer foot wall structure, where a 39  $\Omega$ -m primary layer extends from the surface to 11 m, a 15  $\Omega$ -m secondary layer spans from 11 m to 67 m, and a 22  $\Omega$ -m tertiary layer continues from 67 m onwards.

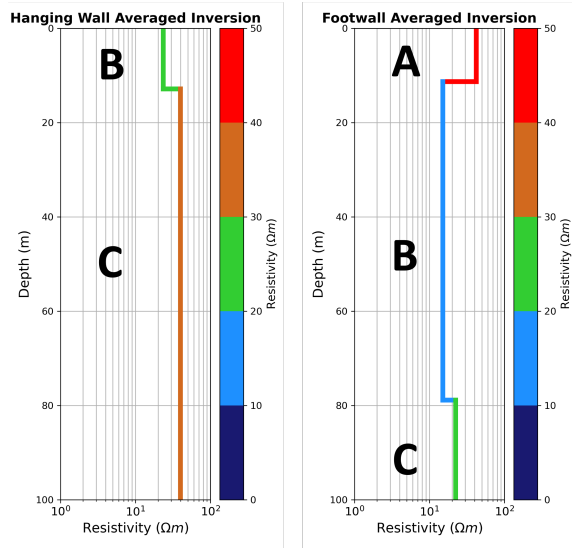


Figure 2: Hanging wall and foot wall averaged inversions near the Howelsen Ski Area fault. Colors indicate the measured resistivity value.

In contrast, a two-layer structure appears in the hanging wall with a 23  $\Omega$ -m primary layer spanning from the surface to 12 m, and a 39  $\Omega$ -m secondary layer continuing from 12 m onwards. These results are summarized in Table 1.

	Layer	$\rho$ ( $\Omega$ -m)	$\rho STD$ ( $\Omega$ -m)	Depth (m)	Depth STD (m)
Foot wall	Layer A	39.3	1.1	11.3	1.3
	Layer B	15.0	1.0	78.8	1.1
	Layer C	22.3	15.0	NA	NA
Hanging wall	Layer B	23.4	1.3	12.8	10
	Layer C	39.7	1.1	NA	NA

Table 1: Observed resistivity, standard deviation of resistivity, depth, and standard deviation of depth values for the hanging wall and foot wall sides of the fault.

### DISCUSSION

In order to reduce the data misfit between observed and predicted data, we performed several inversions, each with a different number of layers in order to assess which layering structure shows the most accurate posterior results. Two, three, and four layer prior models frequently reduced data misfit equally, so we tested all three models and selected the corresponding posterior with the lowest standard deviation. We find that a three-layer structure on the foot wall and two-layer structure on the hanging wall consistently displayed the lowest standard deviation. Figure 2 depicts the average resistivity layers observed on either side of the fault.

Based on USGS geologic maps of the area and observations of the local geology during field work, we expect the electrical resistivity measured at the hanging wall's primary layer to correspond with the electrical resistivity of a deeper layer in the foot wall (Snyder, 1980). However, after observing large amounts of water at the surface of our survey locations, we decided to perform further water saturation analysis before making an interpretation using measured resistivity values alone.

We use Archie's equation to relate the porosity of a rock body to the observed water saturation, the resistivity of water, and our measured bulk resistivity. We estimated an approximate water resistivity value using the 2016-2023 mean May temperature of the Yampa River, as well as the 1976 sum of constituent dissolved solids in the Yampa River (USGS Water Data Support Team, 2023) (United States Geological Survey, 2023). With these two values, we can use the results produced by Schlumberger in Figure 3 to estimate an approximate value for the resistivity of ground water.

Water saturation values were produced based on our observations during survey deployment. We noticed an abundance of water near the surface which can be attributed to a particularly high water table level and thus significant water saturation in the subsurface. In addition, foot wall survey sites tended to be located alongside the Yampa River, so we assumed significant water infiltration in all layers. Foot wall layers A, B, and C were all calculated using a water saturation of  $S_w = 1$ .

The hanging wall situated is situated higher above the Yampa River, and while the surface showed signs of significant water infiltration, we estimated a water saturation of  $S_w = 0.95$  for the top layer and  $S_w = 1$  for the underlying layer. The slightly lower water saturation estimate for the top layer is simply due to the fact that the water table tends to lie deeper below the surface as elevation increases.

## Yampa Valley Cross-fault Geology

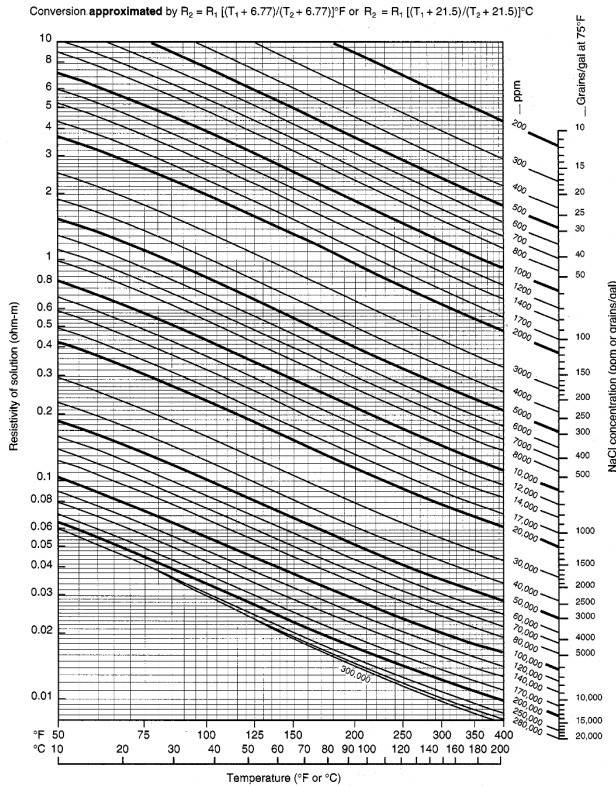


Figure 3: Relationship between temperature, NaCl concentration, and resistivity of water approximated in Schlumberger’s 1997 Log Interpretation Charts publication (Schlumberger, 1997).

Using the values derived above, we solve Archie’s equation for porosity values that account for water saturation, and subsequently introduce a second parameter that helps constrain potential rock types. Estimated values of porosity in addition to our measured resistivities are displayed in Table 2.

	Layer	Resistivity ( $\Omega$ -m)	Porosity (%)
Foot wall	Layer A	39.3	16
	Layer B	15.0	26
	Layer C	22.3	21
Hanging wall	Layer B	23.4	23
	Layer C	39.7	16

Table 2: Observed resistivity and porosity values for the hanging wall and foot wall sides of the fault. By introducing a second parameter (porosity), we are able to better constrain possible interpretations.

After considering both the measured resistivity and porosity values, we suggest that the hanging wall’s first layer (layer B) is predominantly composed of a sandstone shale mixture, while the second layer (layer C) displays properties more akin to pure shale. The foot wall’s second layer (layer B) displays resistivity and porosity values that are consistent with a sandstone/shale mix, and the third layer (layer C) displays charac-

teristics of a shale. We also suggest that the first layer (layer A) of the foot wall is a much younger alluvium deposition created by the presence of the Yampa River. Figure 4 provides a graphical representation of our interpretation of the cross fault geology.

We find that the layers B and C of the hanging wall are highly correlated with layers B and C of the foot wall. Layer A of the foot wall is a geologically recent formation that has been deposited on top of older formations that are consistent across the fault. Because layers B and C appear to be correlated, we suggest that the differences in spring composition may be due to heterogeneity in the alluvial plains or deeper subsurface structures not resolved in our study.

In addition, shallow magnetotelluric (MT) surveys were conducted in May, 2023 near TEM survey locations on the hanging wall. We found that our measured resistivity values were in close agreement with MT observations and likely indicate an abundance of shale in the shallow subsurface of the hanging wall (Howard and McCall, 2023).

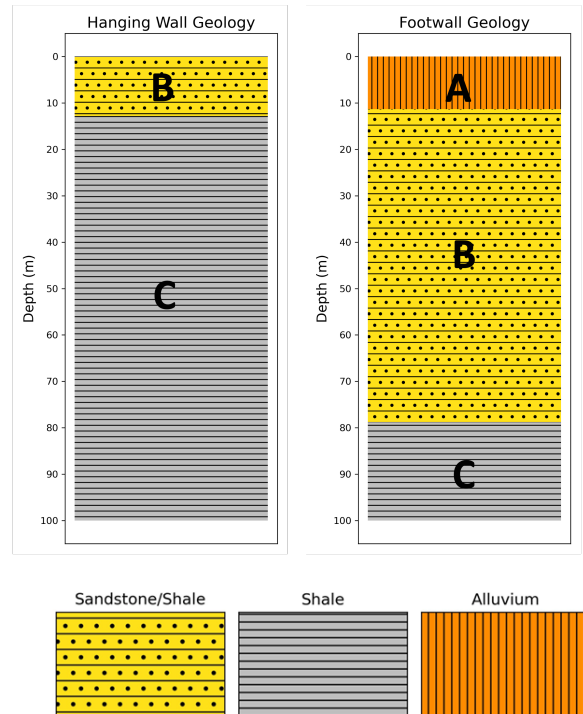


Figure 4: The final interpretation of the geological formations present on the hanging wall and foot wall sides of the Howelsen Ski Area fault. A thin layer of a shale and sandstone mixture overlies a pure shale formation in the Hanging wall. On the foot wall, a geologically recent alluvial deposition sits above a shale and sandstone mixture and another pure shale formation.

## Yampa Valley Cross-fault Geology

### CONCLUSIONS

We provide evidence that the cross-fault geology in the Howelsen Ski Area is highly correlated. Measured values of resistivity and porosity suggest that layers B and C of the hanging wall are similar to layers B and C of the foot wall. Moreover, alluvial depositions on the surface of the foot wall provide a reasonable explanation for the discrepancies in cross-fault surface geology age since these alluvial plains have been created by the presence of the Yampa River in Yampa valley.

To further improve our interpretations of the local lithology, we believe that a water resistivity assessment would be crucial in better estimating porosity values in this area. Knowledge of exact water saturation in survey arrays would also significantly improve porosity calculations and thus better constrain geological interpretations.

Collocated gravimetric measurements may also aid in quantifying the amount of water at survey locations. Moreover, a shallow seismic survey would provide a second method that enables us to interpret rock types and would be beneficial for comparison with the results provided here. Expanded research efforts should focus on the foot wall, since there are significantly fewer TEM sounding locations present in this area.

### AUTHOR STATEMENT

Aljawharah Alangari was responsible for data collection, management, and organization, as well as the production of inversion results in the SPIA software suite. She also lead the lithology analysis and authored the Python code for the lithology visualizations.

Nicholas Dorogy was responsible for data collection, management, and organization. In addition, he produced the averaged cross-fault inversion models, constructed maps of the survey area, and calculated estimations of subsurface porosity.

### ACKNOWLEDGMENTS

We appreciate the monetary contributions made by the Colorado School of Mines Foundation, the Society for Exploration Geophysicists, the geophysical field camp endowment fund, and the Shell Foundation that provide financial support for our research. We would also like to acknowledge the donation of hardware, time, computing resources, and staff members by GTI, Dawson Geophysical, PASSCAL, the United States Geological Survey, the Colorado Geological Survey, and the University of Nevada Reno.

We would like to thank Steamboat Springs Parks & Recreation, Routt County, Jerod Smith from the Colorado State Land Board for granting us permits to our survey location sites, and the Bureau of Land Management Little Snake Field Office for granting us access to public lands in the Emerald Mountain Special Recreation Management Area. We would also like to thank the United Companies and the Tellier family for giving us permission to store the vibroseis trucks on their property.

We extend our gratitude towards Dr. Matthew Siegfried, Dr. Brandon Dugan, Brian Passerella, Dr. Eileen Martin, Dr. Ge Jin, Dr. Jeff Shragge, Dr. Jim Simmons, Dr. Bob Basker, Dr. Todd Fockler, Dr. Paul Sava, Dr. Roy Williams, Dr. Jeff Pepin, Dr. Kyren Bogolub, Dr. Bob Reynolds, Dr. Richie Eperijesi, Melinda Gale, Larry Irons, Jorge Araya, Brett Bernstein, Ahmad Tourei, Ashleigh Miller, Bailey Mullet, Skye Hart, and the 2022 field camp participants for their leadership, time, and assistance with data collection and processing. We particularly appreciate the contributions of Dr. Andrei Swidinsky, Dr. Brandon Dugan, and Brett Bernstein for their support and guidance during data processing.

### APPENDIX A

#### ABEM WALKTEM SURVEY CHARACTERISTICS

Survey parameters were constant across all 22 individual soundings and are outlined in Table 3. The ABEM WalkTEM served as the sole controller for data acquisition. An RC-5 receiver was deployed for the inner receiver, and a larger RC-200 was laid out around the RC-5. We used a standard cable connected to the WalkTEM as the transmitting cable.

ABEM WalkTEM Settings		
Channel No.	Repetition Frequency (Hz)	Current (Amp)
Channel 1	240	0.99
Channel 2	30	7.36
Channel 3	240	0.99
Channel 4	30	7.36
Channel 6	30	0.00
Channel 8	30	0.00

Table 3: Survey design parameters for TEM soundings.

# Yampa Valley Cross-fault Geology

## APPENDIX B

### INDIVIDUAL INVERSION RESULTS

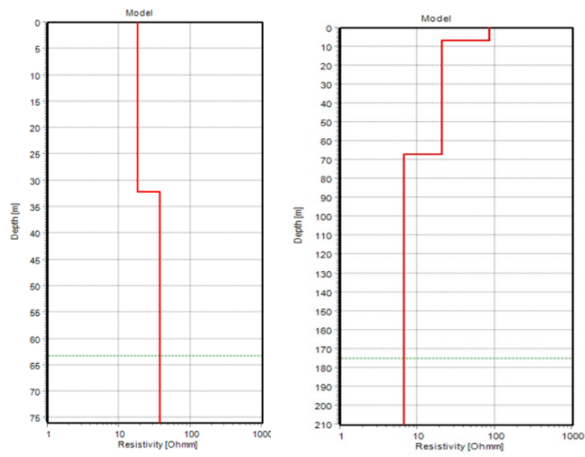


Figure B-1: Example individual inversion results of the hanging wall (left) and foot wall (right).

## Yampa Valley Cross-fault Geology

### REFERENCES

- AAPG Wiki, 2023, Archie equation: [https://wiki.aapg.org/Archie\\_equation](https://wiki.aapg.org/Archie_equation). (Accessed on : June 9, 2023).
- Aarhus SPIA Development Team, 2023, Aarhus spia: Seismic processing in action. Aarhus University.
- Archie, G. E., 1952, Classification of carbonate reservoir rocks and petrophysical considerations: AAPG Bulletin, **36**, 218–298.
- Christopherson, K. R., 1997, A geophysical study of the steamboat springs, colorado geothermal systems: PhD thesis, University of Colorado.
- Howard, J., and J. McCall, 2023, Shallow magnetotelluric soundings of the steamboat basin and north park, colorado: PhD thesis, Colorado School of Mines.
- Schlumberger, 1997, Log interpretation charts: Schlumberger Wireline & Testing.
- Snyder, G. L., 1980, Geologic map of the northernmost gore range and southernmost northern park range, grand, jackson, and routt counties, colorado: Department of the Interior United States Geological Survey. (Map, 1:48000).
- United States Geological Survey, 2023, Yampa river at steamboat springs, co - 09239500: <https://waterdata.usgs.gov/monitoring-location/09239500/parameterCode=00010period=P200D>. (Accessed on: June 9, 2023).
- USGS Water Data Support Team, 2023, Water quality samples for usa: Sample data: [https://nwis.waterdata.usgs.gov/usa/nwis/qwdata/?site\\_no=402918106502700agency\\_cd=USGSinventory\\_output=Ordbinventory\\_output=fileTZoutput=0pmcdcompare=Greater](https://nwis.waterdata.usgs.gov/usa/nwis/qwdata/?site_no=402918106502700agency_cd=USGSinventory_output=Ordbinventory_output=fileTZoutput=0pmcdcompare=Greater) (Accessed on : June 9, 2023).